J Nanostruct 16(2): 1678-1685, Spring 2026

RESEARCH PAPER

Investigations Structural, Optical and Morphological of Ag-Doped SnS Thin Films

Manal Dakhil Sakhil

Faculty of Physical Education and Sports Sciences, University of Kerbala, Iraq

ARTICLE INFO

Article History:
Received 08 December 2025
Accepted 05 March 2026
Published 01 April 2026

Keywords:
AFM
Optical properties
SnS/Ag thin films
XRD

ABSTRACT

Tin sulfide (SnS) and silver (Ag)-doped SnS films were synthesized using chemical spray pyrolysis with Ag concentrations of 0%, 2%, and 4%. XRD analysis confirmed an orthorhombic structure, emphasizing the (021) plane. Crystallite size increased from 12.98 nm to 14.87 nm with Ag doping. Interestingly, the average particle size grew to 52.36 nm at 2% Ag doping, but decreased to 47.46 nm at 4%. As Ag content increased, the band edge shifted to lower energy, coupled with optical band gap fluctuated between 1.46 eV to 1.36 eV. Refractive index (n) and absorption coefficient (α) values were in the range of 3.3 to 3.5 and 1×10^4 cm^-1 to 4×10^4 cm^-1, respectively. This study highlights the structural and optical changes induced by Ag doping, providing valuable insights for potential applications.

How to cite this article
Dakhil Sakhil M. Investigations Structural, Optical and Morphological of Ag-Doped SnS Thin Films. J Nanostruct, 2026; 16(2):1678-1685. DOI: 10.22052/JNS.2026.02.020

INTRODUCTION

Researchers have focused on binary semiconductor compounds like SnS, SnSe, Cu2S, ZnS for advanced solar cell applications [1,2]. SnS semiconductor belonging to the IV-VI group, is engaged in the field of solar energy, exhibiting dual conductivity types (both p-type and n-type) in need of tin, sulfur content, and annealing temperature [3,4]. With a direct bandgap of (~1.3) eV and an indirect bandgap ranging from 1.0 to 1.2 eV [5,6], SnS holds promise for efficient solar cells. Its orthorhombic crystal structure features each Sn atom surrounded by six S atoms, forming short and long SnS bonds with interatomic spacings of 2.7 Å and 3.4 Å, respectively. [7]. Several deposition techniques, among them chemical spray pyrolysis, have been employed to fabricate SnS films, both in their pristine form and with intentional doping [8The chemical spray pyrolysis method was chosen to deposit SnS films due to its simplicity and cost-effectiveness [9-10]. Critical parameters, such as base temperature, precursor ratios, solvent type, and spray rate, part in the process of deciding the physical properties of the films [11-12]. Among these factors, substrate temperature stands out as the most influential parameter.[13]. In found in this research, SnS and Ag-doped SnS films were produced via chemical spray pyrolysis, a cost-effective and straightforward technique, to investigate the physical properties of SnS:Ag.

MATERIALS AND METHODS

Reliable thin films of SnS and SnS:Ag were fabricated through a lab-built spray pyrolysis coating process. Precursors, consisting of 0.1 M $SnCl_2 \bullet 2H_2O$ and thiourea dissolved in deionized water, were utilized, and Ag doping levels (0%,

* *Corresponding Author Email: manal.dakhil@uokerbala.edu.iq*

2%, 4%) were introduced by incorporating silver trichloride ($AgCl_3$) in isopropyl alcohol. The optimized deposition conditions included a substrate temperature of 450°C, a spout-base distance of 29 cm, a 9-second spraying period followed by an 85-second interval, and a spray rate of 5 mL/min. The film thickness, determined through a weighing method, was measured at 340 ± 25 nm. UV-visible spectroscopy captured optical transmittance spectra within the range of 300–900 nm. Film structure was examined through XRD, and the surface was characterized using AFM.

Characterization

XRD

Fig. 1 presents the XRD spectra, indicating the characteristics of the deposited films. The broad reflectance of XRD peaks in the as-prepared thin films suggests a small particle size. Notably, peaks at 22.25°, 27.24°, 48.78°, and 67.75° correspond to (110), (021), (211), and (080) planes, respectively, consistent with SnS and in accordance with ICDD card no. (39-0354), highlighting a strong presence of the (021) plane. The heightened Bragg peaks suggest improved crystallinity, potentially attributed to the introduction of nucleating centers through doping [14,15]. Crystallite size calculations were conducted using Scherer's equation [16,17].

$$D = \frac{0.9\lambda}{\beta\cos\theta} \quad (1)$$

The pure SnS sample displays a crystallite size of 12.98 nm, whereas the 2% Ag-doped SnS thin films show a particle size of 13.86 nm, and the 4% Ag-doped SnS thin film has a crystallite size of 14.87 nm. The diversity in crystallite size is likely linked to lattice dilatation [18].

Dislocation density (δ) and microstrain (ε) were determined using Eqs. 2 and 3 [19, 20]:

$$\delta = \frac{1}{D^2} \quad (2)$$

$$\varepsilon = \frac{\beta\cos\theta}{4} \quad (3)$$

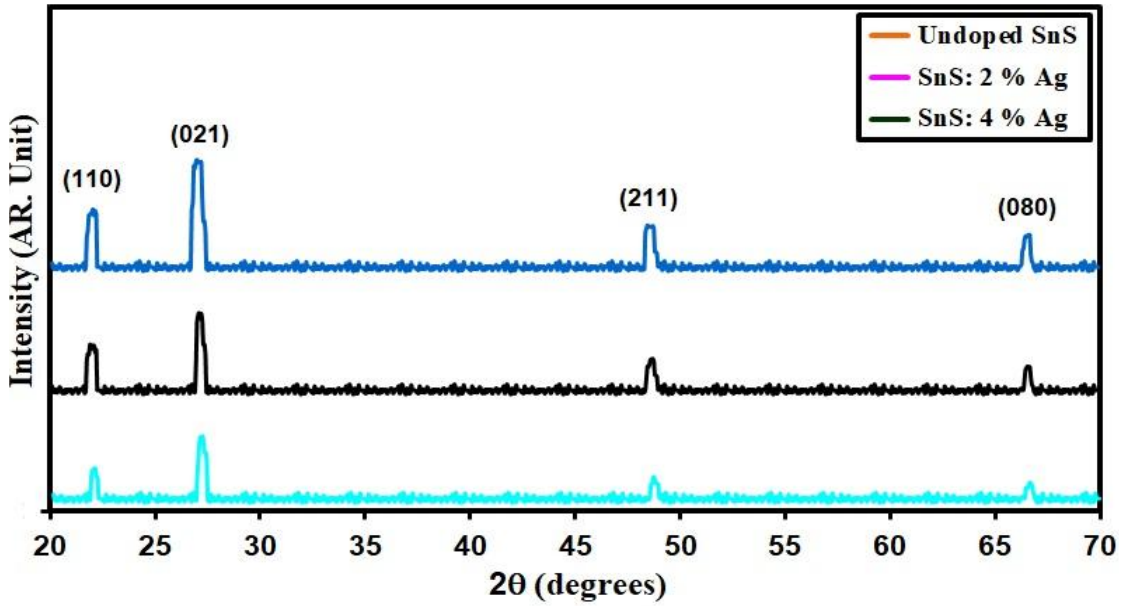

Fig. 1. XRD pattern of the intended films.

Table 1. Summary of the the films' structural characteristics under consideration.

Samples	2θ (°)	(hkl) Plane	FWHM (°)	crystallite size (nm)	Optical bandgap (eV)	Dislocations density ($\times 10^{14}$) (lines/m^2)	Strain $\times 10^{-4}$
Undoped SnS	27.45	021	0.63	12.98	1.46	59.35	26.70
SnS: 2% Ag	27.42	021	0.59	13.86	1.41	52.05	25.00
SnS: 4% Ag	27.39	021	0.55	14.87	1.36	45.22	23.31

The value of δ was 4.52×10^{15} lines/m^2 and ε was 23.31×10^{-4} for Ag content of 4 at%. (Table 1).

AFM Analysis

AFM was employed to assess the topography of both SnS and Ag-doped SnS. The 2-D images illustrate film surfaces, providing insights into particle size (Aps) and surface roughness (RMS). Fig. 3 presents AFM images of SnS analyzed over a 78nm x 78nm area. The films exhibit a uniform morphology with an irregular surface structure, featuring varying surface roughness and densely packed grains. The average particle size (Aps) is larger for films prepared without Ag doping. In Ag-doped films, Aps decreases to 52.36nm with a 2% doping concentration, and further increments to 4% lead to a decrease to 47.46nm. These findings align with references [21,22]. Fig. 3 and Table 2

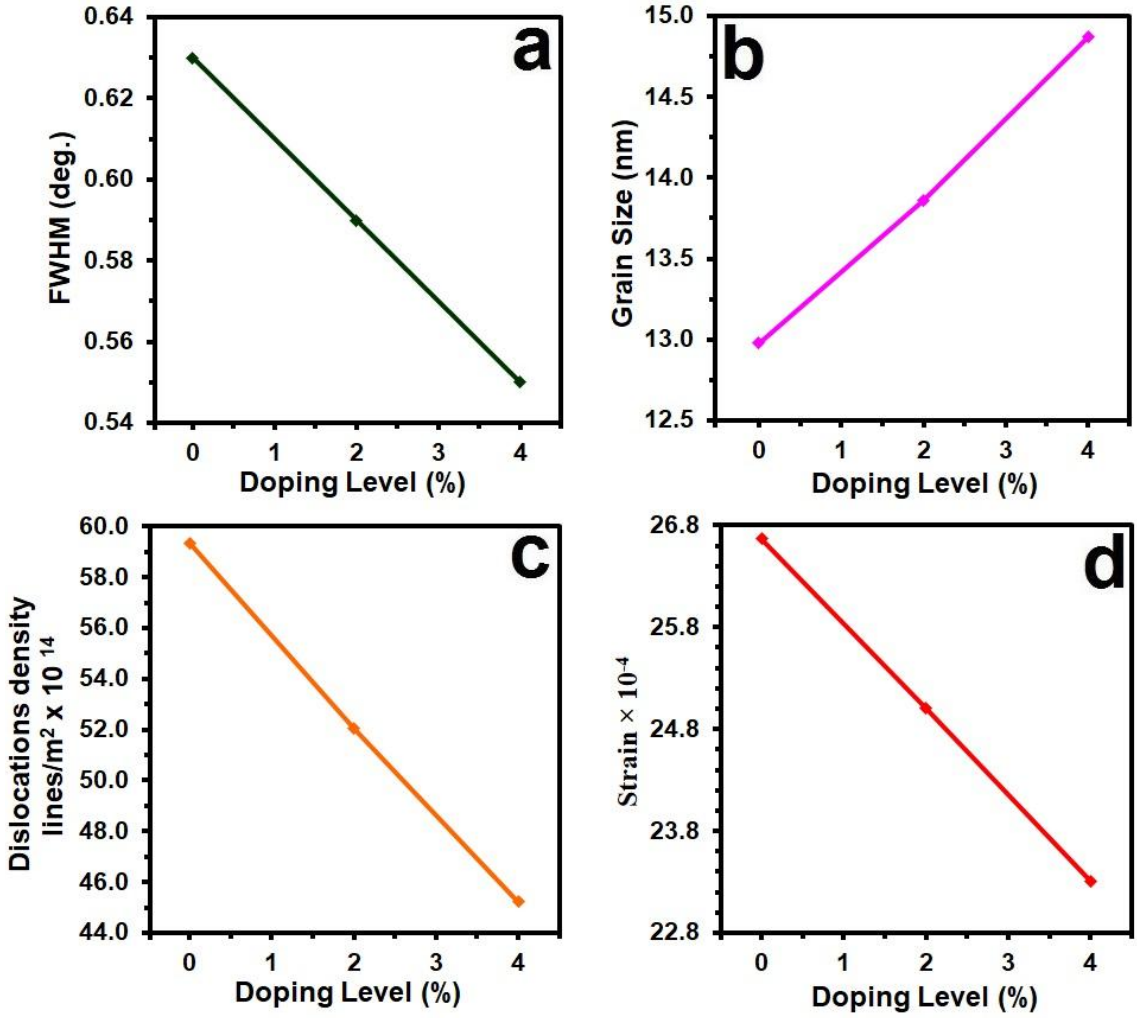

Fig. 2. FWHM, strain and dislocation of pure and SnS: Ag films with different dopant.

Table 2. Morphological parameters (AFM) of SnS thin films as a function of Ag doping concentration.

Samples	A_{ps} nm	Ra (nm)	RMS (nm)
Undoped SnS	60.11	6.77	7.35
SnS: 2% Ag	52.36	5.69	6.58
SnS: 4% Ag	47.46	4.29	5.36

present the AFM parameters.

Optical Analysis

Fig. 4 shows transmittance (T%) curves, indicating highly transparent films with an average value surpassing 70% in the visible range. With increasing Ag concentration, transmission decreases, and the absorption edge shifts towards higher wavelengths [23].

To calculate the absorption coefficient (α) at

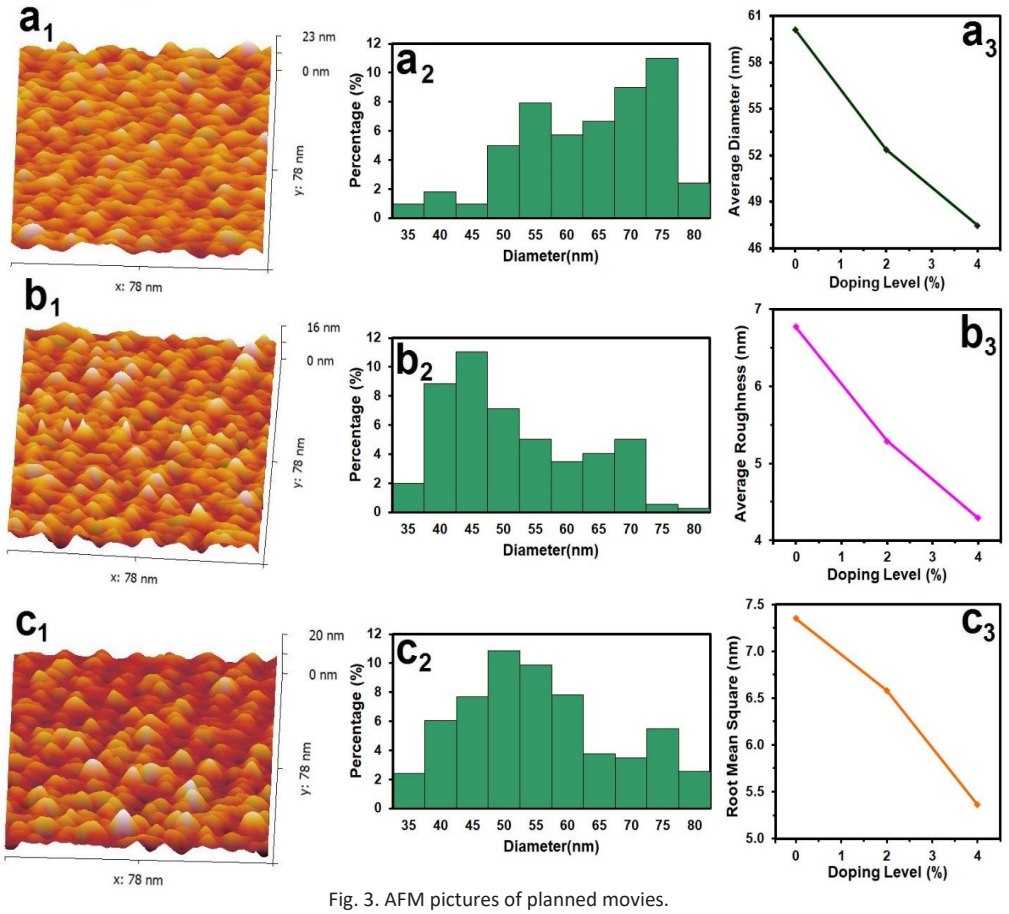

Fig. 3. AFM pictures of planned movies.

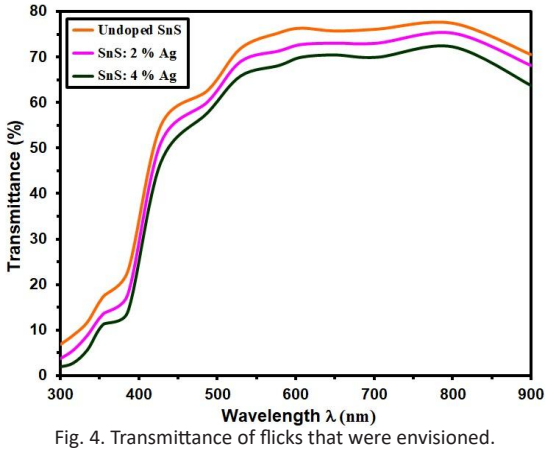

Fig. 4. Transmittance of flicks that were envisioned.

film thickness (d) Eq.4. [24, 25] are used:

$$\alpha = \frac{\ln(1/T)}{d} \quad (4)$$

The values of α is offered in Fig. 5. These values are varied between $1\times10^4 cm^{-1}$and 4×10^4 cm^{-1}.

The energy band gap (Eg) was determined using the derived relationship [26, 27].

$$(\alpha h\nu)^2 = A(h\nu - E_g) \quad (5)$$

The equation includes a proportionality constant represented by A. Fig. 6 depicts a decrease in bandgap (Eg) values from 1.46 eV to 1.36 eV for films doped with 2 at% Ag. A slight additional decrease is observed with higher doping, attributed to the band shrinkage effect resulting from an increase in carrier concentration. [28].

The extinction coefficient (k) was calculated using Eq. 6 [29- 30]:

$$K = \frac{\alpha\lambda}{4\pi} \quad (6)$$

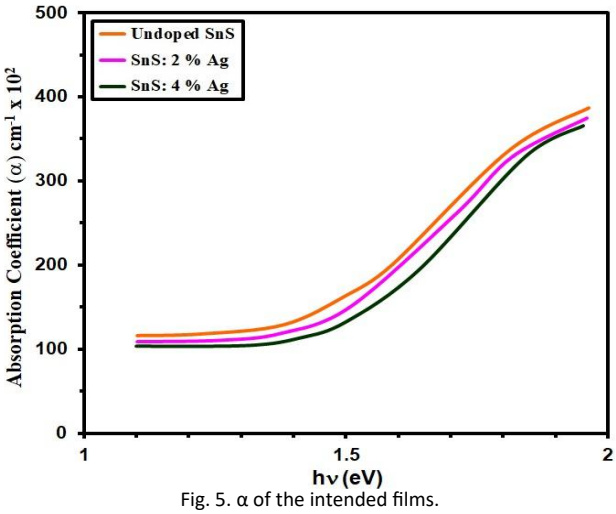

Fig. 5. α of the intended films.

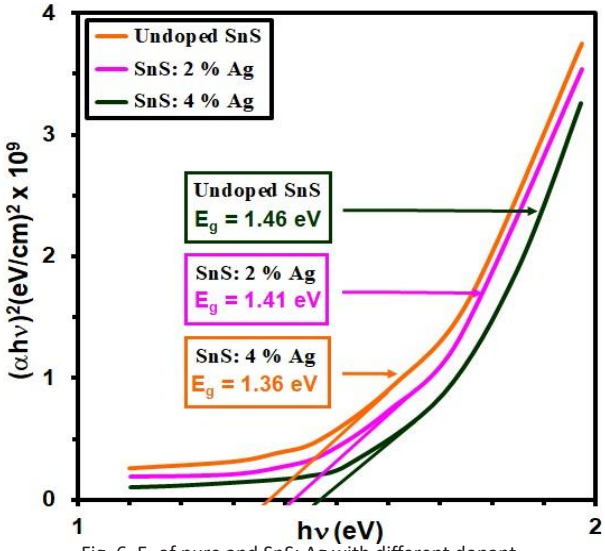

Fig. 6. E_g of pure and SnS: Ag with different dopant.

The decrease in α with an increase in film doping content is associated with fluctuations in the crystallite size of the films [31].

In Fig. 7, the extinction coefficient (k) demonstrates a significant decline as the wavelength ranges from 450 nm to 600 nm. The low values of (k) suggest a film surface that is smooth and uniform [32].

The refractive index (n) was determined at various wavelengths using optical reflectivity (R) and the relationship given by Eq. 7 [33-34].

$$n = \frac{1 + R^{\frac{1}{2}}}{1 - R^{\frac{1}{2}}} \quad (7)$$

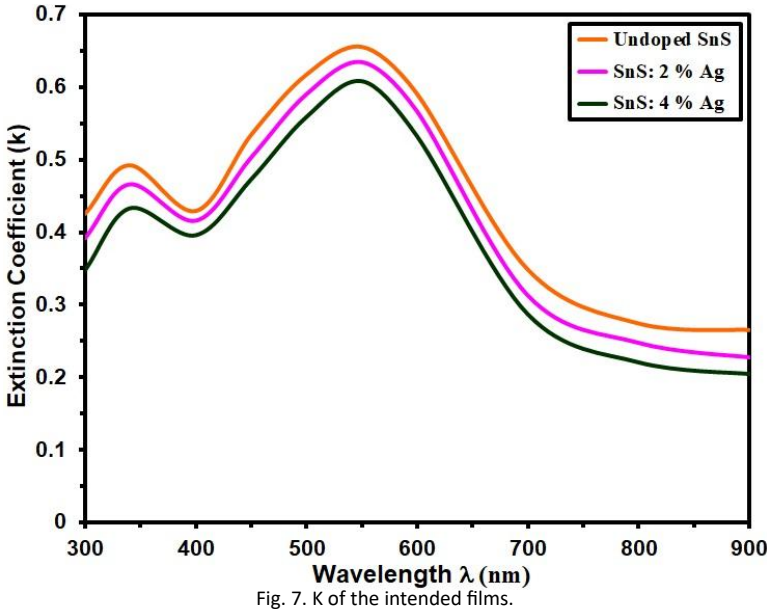

Fig. 7. K of the intended films.

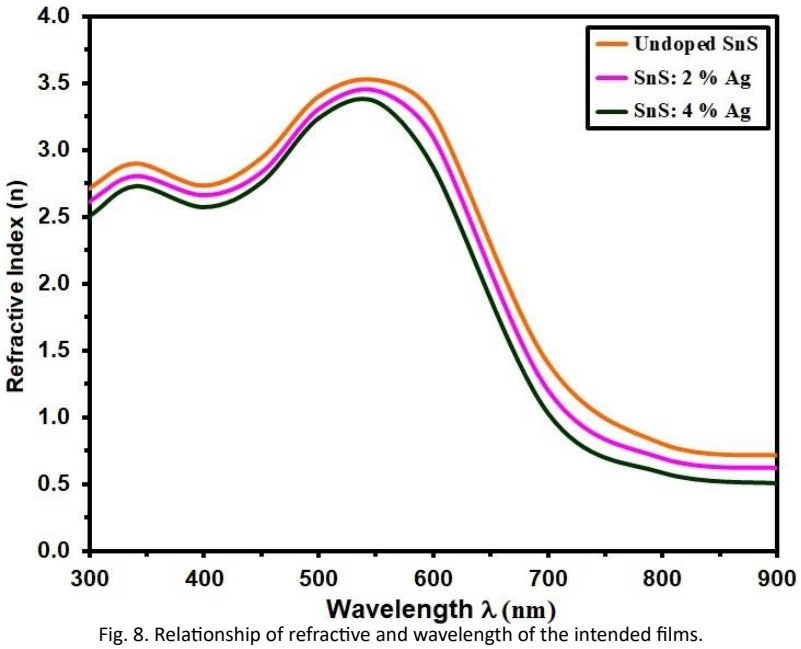

Fig. 8. Relationship of refractive and wavelength of the intended films.

The variation of (n) is shown in Fig. 8. Due to Ag doping, a clear shift in maximum value of (n) to the higher wavelength region that can be easily noted [35].

CONCLUSION

SnS: Ag thin films were synthesized by spray pyrolysis, all films were polycrystalline also, the crystallinity was enhanced with doping ratio of 4 %. The band gap was seen in the area of (1.46-1.36) eV. Diffraction peaks were obtained. These peaks were confirming to orthorhombic SnS was observed with identified (021) plane. Average Particle size and surface roughness are studied by AFM and found to be decreased due to silver doping.

CONFLICT OF INTEREST

The authors declare that there is no conflict of interests regarding the publication of this manuscript.

REFERENCES

1. Sajeesh TH, Warrier AR, Kartha CS, Vijayakumar KP. Optimization of parameters of chemical spray pyrolysis technique to get n and p-type layers of SnS. Thin Solid Films. 2010;518(15):4370-4374.
2. El-Nahass MM, Zeyada HM, Aziz MS, El-Ghamaz NA. Optical properties of thermally evaporated SnS thin films. Opt Mater. 2002;20(3):159-170.
3. Yago A, Sasagawa S, Akaki Y, Nakamura S, Oomae H, Katagiri H, et al. Comparison of buffer layers on SnS thin-film solar cells prepared by co-evaporation. physica status solidi c. 2017;14(6).
4. Banai RE, Horn MW, Brownson JRS. A review of tin (II) monosulfide and its potential as a photovoltaic absorber. Sol Energy Mater Sol Cells. 2016;150:112-129.
5. Banai RE, Lee H, Tanen NJ, Urena RE, Cordell JJ, Horn MW, et al. Investigation of RF-sputtered tin sulfide thin films with in situ heating for photovoltaic applications. 2014 IEEE 40th Photovoltaic Specialist Conference (PVSC); 2014/06: IEEE; 2014. p. 0290-0294.
6. Ramasamy K, Kuznetsov VL, Gopal K, Malik MA, Raftery J, Edwards PP, et al. Organotin Dithiocarbamates: Single-Source Precursors for Tin Sulfide Thin Films by Aerosol-Assisted Chemical Vapor Deposition (AACVD). Chem Mater. 2013;25(3):266-276.
7. Sun J, Huang Y, Nie S, Chen Z, Xu J, Zhao L, et al. Improved mobility of sol-gel method processed transparent tin sulfide thin films. Mater Lett. 2016;178:231-234.
8. Jamali-Sheini F, Niknia F, Cheraghizade M, Yousefi R, Mahmoudian MR. Broad Spectral Response of Se-Doped SnS Nanorods Synthesized through Electrodeposition. ChemElectroChem. 2017;4(6):1478-1486.
9. Santhosh Kumar K, Manoharan C, Dhanapandian S, Gowri Manohari A, Mahalingam T. Effect of indium incorporation on properties of SnS thin films prepared by spray pyrolysis. Optik. 2014;125(15):3996-4000.
10. Javed A, Qurat ul A, Bashir M. Controlled growth, structure and optical properties of Fe-doped cubic π- SnS thin films. J Alloys Compd. 2018;759:14-21.
11. Price LS, Parkin IP, Hardy AME, Clark RJH, Hibbert TG, Molloy KC. Atmospheric Pressure Chemical Vapor Deposition of Tin Sulfides (SnS, Sn_2S_3, and SnS_2) on Glass. Chem Mater. 1999;11(7):1792-1799.
12. Ray SC, Karanjai MK, DasGupta D. Structure and photoconductive properties of dip-deposited SnS and SnS2 thin films and their conversion to tin dioxide by annealing in air. Thin Solid Films. 1999;350(1-2):72-78.
13. Santhosh Kumar K, Manoharan C, Dhanapandian S, Gowri Manohari A. Effect of Sb dopant on the structural, optical and electrical properties of SnS thin films by spray pyrolysis technique. Spectrochimica Acta Part A: Molecular and Biomolecular Spectroscopy. 2013;115:840-844.
14. Hassan ES, Mubarak TH, Chiad SS, Habubi NF, Khadayeir AA, Dawood MO, et al. Physical Properties of indium doped Cadmium sulfide thin films prepared by (SPT). Journal of Physics: Conference Series. 2019;1294(2):022008.
15. Othman MS, Mishjil KA, Rashid HG, Chiad SS, Habubi NF, Al-Baidhany IA. Comparison of the structure, electronic, and optical behaviors of tin-doped CdO alloys and thin films. Journal of Materials Science: Materials in Electronics. 2020;31(11):9037-9043.
16. Paraguay D F, Morales J, Estrada L W, Andrade E, Miki-Yoshida M. Influence of Al, In, Cu, Fe and Sn dopants in the microstructure of zinc oxide thin films obtained by spray pyrolysis. Thin Solid Films. 2000;366(1-2):16-27.
17. Williamson GK, Smallman RE. III. Dislocation densities in some annealed and cold-worked metals from measurements on the X-ray debye-scherrer spectrum. Philos Mag. 1956;1(1):34-46.
18. Santhosh Kumar K, Gowri Manohari A, Lou C, Mahalingam T, Dhanapandian S. Influence of Cu dopant on the optical and electrical properties of spray deposited tin sulphide thin films. Vacuum. 2016;128:226-229.
19. Jandow NN, Othman MS, Habubi NF, Chiad SS, Mishjil KA, Al-Baidhany IA. Theoretical and experimental investigation of structural and optical properties of lithium doped cadmium oxide thin films. Materials Research Express. 2019;6(11):116434.
20. Hassan ES, Qader KY, Hadi EH, Chiad SS, Habubi NF, Abass KH. Sensitivity of Nanostructured Mn-Doped Cobalt Oxide Films for Gas Sensor Application. Nano Biomed Eng. 2020;12(3).
21. Reghima M, Akkari A, Guasch C, Kamoun-Turki N. Structural, Optical, and Electrical Properties of SnS:Ag Thin Films. J Electron Mater. 2015;44(11):4392-4399.
22. Baby BH, Bharathi Mohan D. Structural, optical and electrical studies of DC-RF magnetron co-sputtered Cu, In and Ag doped SnS thin films for photovoltaic applications. Solar Energy. 2019;194:61-73.
23. Minami T, Kakumu T, Takeda Y, Takata S. Highly transparent and conductive ZnO:In_2O_3 thin films prepared by d.c. magnetron sputtering. Thin Solid Films. 1996;290-291:1-5.
24. Hassan ES, Razzaq ZS, Qutbi HAS, Chiad SS, Habubi NF, Abass KH. Sensitivity of Cadmium Sulfide under the Influence of Both Substrate Temperature and Gas Operation. Nano Biomed Eng. 2021;13(4).
25. Khadayeir AA, Hassan ES, Mubarak TH, Chiad SS, Habubi NF, Dawood MO, et al. The effect of substrate temperature on the physical properties of copper oxide films. Journal of

Physics: Conference Series. 2019;1294(2):022009.
26. Ahmed NY. Effect of Boron on Structural, Optical Characterization of Nanostructured Fe_2O_3 thin Films. Neuroquantology. 2020;18(6):55-60.
27. Ghazai AJ, Abdulmunem OM, Qader KY, Chiad SS, Habubi NF. Investigation of some physical properties of Mn doped ZnS nano thin films. AIP Conference Proceedings: AIP Publishing; 2020. p. 020101.
28. Ong HC, Zhu AXE, Du GT. Dependence of the excitonic transition energies and mosaicity on residual strain in ZnO thin films. Appl Phys Lett. 2002;80(6):941-943.
29. Sakhil MD. Influence MgO Dopant on Structural and Optical Properties of Nanostructured CuO Thin Films. Neuroquantology. 2020;18(5):56-61.
30. Review for "Enhancing Oxygen Evolution Reaction Performance via Zn/Fe Co-Doping in Co_3O_4 Nanostructure: Mechanistic Insights and Surface Reconstruction Dynamics". Royal Society of Chemistry (RSC); 2025.
31. Kafashan H, Ebrahimi-Kahrizsangi R, Jamali-Sheini F, Yousefi R. Effect of Al doping on the structural and optical properties of electrodeposited SnS thin films. physica status solidi (a). 2016;213(5):1302-1308.
32. Rusu GI, Popa ME, Rusu GG, Salaoru I. On the electronic transport properties of polycrystalline ZnSe films. Appl Surf Sci. 2003;218(1-4):223-231.
33. Khadayeir AA, Hassan ES, Chiad SS, Habubi NF, Abass KH, Rahid MH, et al. Structural and Optical Properties of Boron Doped Cadmium Oxide. Journal of Physics: Conference Series. 2019;1234(1):012014.
34. Sharba KS. Enhancement of Urbach Energy and Dispersion Parameters of Polyvinyl Alcohol with Kaolin Additive. Neuroquantology. 2020;18(3):66-73.
35. Ali RS. Characterization of ZnO Thin Film/p-Si Fabricated by Vacuum Evaporation Method for Solar Cell Applications. Neuroquantology. 2020;18(1):26-31.